Estuaries Vol. 26, No. 6, p. 1437–1449 December 2003

On the Linkages Among Density, Flow, and Bathymetry Gradients at the Entrance to the Chesapeake Bay

ARNOLDO VALLE-LEVINSON[1,*], WILLIAM C. BOICOURT[2], and MICHAEL R. ROMAN[2]

[1] *Center for Coastal Physical Oceanography, Department of Ocean, Earth, and Atmospheric Sciences, Crittenton Hall, Old Dominion University, Norfolk, Virginia 23529*

[2] *Horn Point Laboratory, University of Maryland Center for Environmental Science, P. O. Box 775, Cambridge, Maryland 21613*

ABSTRACT: Linkages among density, flow, and bathymetry gradients were explored at the entrance to the Chesapeake Bay with underway measurements of density and flow profiles. Four tidal cycles were sampled along a transect that crossed the bay entrance during cruises in April–May of 1997 and in July of 1997. The April–May cruise coincided with neap tides, while the July cruise occurred during spring tides. The bathymetry of the bay entrance transect featured a broad Chesapeake Channel, 8 km wide and 17 m deep, and a narrow North Channel, 2 km wide and 14 m deep. The two channels were separated by an area with typical depths of 7 m. Linkages among flows, bathymetry, and water density were best established over the North Channel during both cruises. Over this channel, greatest convergence rates alternated from the left (looking into the estuary) slope of the channel during ebb to the right slope during flood as a result of the coupling between bathymetry and tidal flow through bottom friction. These convergences were linked to the strongest transverse shears in the along-estuary tidal flow and to the appearance of salinity fronts, most markedly during ebb periods. In the wide channel, the Chesapeake Channel, frontogenesis mechanisms over the northern slope of the channel were similar to those in the North Channel only in July, when buoyancy was relatively weak and tidal forcing was relatively strong. In April–May, when buoyancy was relatively large and tidal forcing was relatively weak, the recurrence of fronts over the same northern slope of the Chesapeake Channel was independent of the tidal phase. The distinct frontogenesis in the Chesapeake Channel during the increased buoyancy period was attributed to a strong pycnocline that insulated the surface tidal flow from the effects of bottom friction, which tends to decrease the strength of the tidal flow over relatively shallow areas.

Introduction

Studies on the linkage between density gradients and flow gradients have usually concentrated on tidal intrusion fronts and plume fronts (e.g., Garvine 1974; Luketina and Imberger 1989; Marmorino and Trump 1996; O'Donnell 1997; O'Donnell et al. 1998). A third type of fronts, the along-estuary or axial fronts (O'Donnell 1993), tends to be linked to bathymetric gradients. The formation of axial fronts has been explained only during flood tides (e.g., Nunes and Simpson 1985; Simpson and Turrell 1986; Huzzey and Brubaker 1988; Brown et al. 1991; Turrell et al. 1996) by invoking the mechanism of differential advection of the along-estuary density field by the laterally sheared along-estuary flow. This mechanism is thought to allow the development of surface transverse circulation from either bank of the estuary that causes axial convergences along the middle of the channel or thalweg. The same mechanism has been used in various studies (Sarabun 1980; Huzzey and Bubaker 1988; Swift et al. 1996) to explain observations of late-flood axial convergence that actually appeared over the edge, not in the middle of the channel. Most of the studies suggested that density gradients are crucial for the development of transverse circulation associated with axial convergences. These are reasonable explanations for convergences that appear during late flood stages, but cannot be used to explain along-estuary convergences during ebb stages as observed by Sarabun (1980), Ferrier and Anderson (1997), and Valle-Levinson et al. (2000).

The development of convergences over the channel edges is also ubiquitous in the lower Chesapeake Bay (e.g., Sletten et al. 1999), the James River (Valle-Levinson et al. 2000), and in coastal lagoons with weak density gradients (Valle-Levinson unpublished data). Supported by observations in the James River and by results from an analytic model, Valle-Levinson et al. (2000) proposed that the location and timing of along-estuary convergences was primarily determined by the interaction between bathymetry and tidal flow. They postulated that density gradients may contribute to strengthen the convergences but not to form them. The objectives of the present study are to

* Corresponding author: tele: 757/683-5578; fax: 757/683-5550; e-mail: arnoldo@ccpo.odu.edu

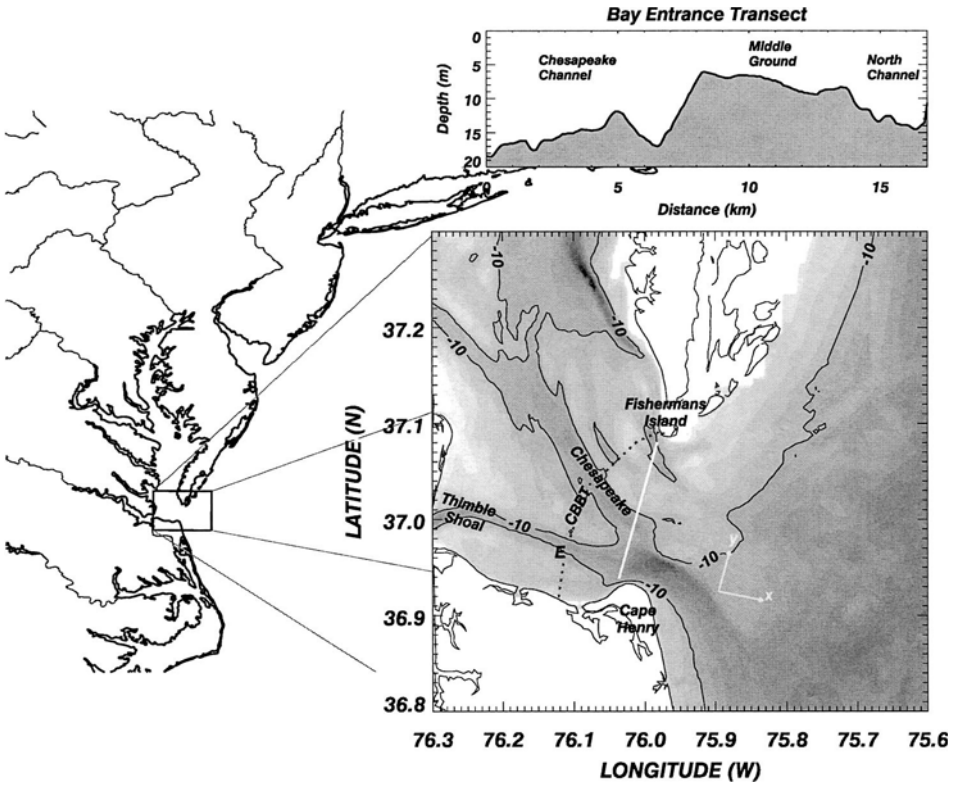

Fig. 1. Map of the study area in the lower Chesapeake Bay showing the transect sampled as the white line between Cape Henry and Fishermans Island. The bathymetry is shown in shaded contours at intervals of 2.5 m and with labels for the Chesapeake and Thimble Shoal Channels. The Chesapeake Bay Bridge Tunnel (CBBT) is represented by the black dotted line and E indicates the CBBT location for wind velocity and sea level measurements. A cross-section (looking into the estuary) of the transect sampled is shown in the upper panel.

extend the results of Valle-Levinson et al. (2000) by documenting the linkage of flow and density gradients to bathymetry gradients during both stages of the tidal cycle in the lower Chesapeake Bay, and proposing the dynamic underpinnings of these linkages.

Study Area

The lower Chesapeake Bay is representative of wide, partially mixed coastal plain estuaries with a characteristic channel and shoals cross-sectional bathymetry (Fig. 1). Physical oceanographic processes in the lower Chesapeake Bay are chiefly influenced by bathymetry, wind, tidal, and buoyancy forcing. Despite the fact that the transect studied here is only approximately 2 km landward of that presented by Valle-Levinson et al. (1998), its bathymetry is decisively different. The portion of the bay studied here includes the confluence between the Chesapeake Channel and the Thimble Shoal Channel. This junction depicts a broad bathymetric depression at least 8 km wide, with a maximum depth of 17 m (Fig. 1). Immediately to the north of this juncture the bathymetry shoals rapidly to 6–7 m within the 6-km wide Middle Ground. Between Middle Ground and Fishermans Island lies the North Channel, with depths of 14 m that compare to those at the confluence of Chesapeake and Thimble Shoal Channels and roughly double the typical depth of Middle Ground.

Wind forcing in the lower Chesapeake Bay is seasonal and primarily from the northeast and southwest (Paraso and Valle-Levinson 1996). Northeasterly winds prevail from late summer to early spring, while southwesterly winds dominate during the summer. During any season, strong winds can occur from either direction. The most energetic wind events are usually from the northeast or northwest during late fall and winter, although southwesterly winds can occasionally be very energetic.

Tidal forcing in the lower Chesapeake Bay is predominantly semidiurnal (Browne and Fisher 1988). The interaction among the three semidiurnal tidal constituents (M_2, N_2, and S_2) generates fortnightly and monthly variability in the tidal currents. Owing to the fact that the N_2 constituent dominates over the S_2 in the lower bay, there is a marked asymmetry between consecutive spring (or

neap) tides thus causing a primary and a secondary spring (or neap) tide during one month. During spring tides, the currents in the lower bay may exceed 1 m s^{-1}.

Buoyancy forcing to the lower Chesapeake Bay is dominated by river discharge. River discharge peaks during the months of March and April and is least during August and September. The mean surface salinity is lowest throughout the bay in the April–May period and highest in September–November, roughly 1 mo after the river discharge extremes. The present study was conducted under neap and spring tides, relatively weak wind forcing, and during high and moderate buoyancy forcing.

Data Collection and Processing

The data collection consisted of repeating a 17-km-long cross-estuary transect to capture the intratidal variability of the distribution of the flow and density fields across the entrance to the Chesapeake Bay (Fig. 1). The cross-estuary transect was sampled throughout nearly four semidiurnal tidal cycles, first in the spring of 1997 and then in the summer of 1997. The spring cruise was done April 29–May 1, 1997, at neap tides. The summer cruise took place July 20–22, 1997, during secondary spring tides. These cruises were aboard the R/V *Cape Henlopen*.

Each of the two cruises included records of underway current and density profiles, and of surface temperature and salinity values. This sampling strategy allowed calculation of horizontal gradients of density and flow, and determination of the vertical structure of properties where the gradients were most intense. Velocity data were obtained with a 614.4 kHz Broad Band RD Instruments Acoustic Doppler Current Profiler (ADCP). The ADCP was mounted looking downward on a small (1.2 m long) catamaran and towed to the starboard side of the ship at speeds of approximately 2.5 m s^{-1}. Velocity profiles were recorded at intervals of 5 s and averaged over 30 seconds, which gave a horizontal spatial resolution of about 75 m. The bin size for vertical resolution was 0.5 m and the closest bin to the surface was located at a depth of nearly 2 m. These settings yielded an accuracy of 0.01 m s^{-1} in the measured velocities. Compass calibration and data correction were performed following Joyce (1989) with navigation recorded through a Trimble Differential Global Positioning System.

At the same time that the ADCP was being towed, water temperature and salinity profiles were being acquired with a Seabird SBE-19 Conductivity-Temperature-Depth (CTD) recorder mounted in an undulating towed body Scanfish MK II. The Scanfish was towed from the port side of the ship and undulated at vertical rates of 0.5 m s^{-1} within 2 m from the surface and bottom. This yielded minimum horizontal resolutions of 200 m and a typical vertical resolution of 0.25 m as the sampling frequency of the CTD was 2 Hz. The separation between the ADCP and the undulating CTD was approximately 50 m at the surface and was taken into account to correct the location of each measurement recorded by the CTD. Near-surface temperature and salinity values (at approximately 1 m depth) were recorded with a Sea Bird SBE-1621 thermosalinograph. The thermosalinograph recorded one value every 10 s—i.e., it provided a spatial resolution of 25 m.

The towing speed of 2.5 m s^{-1} allowed coverage of the 17-km transect in 2 h. By the end of each cruise, the transect at the bay entrance was occupied 24 times. The current velocity data at each of the 24 transects were rotated by 11°T to coincide with a reference frame in which the direction perpendicular to the entrance of the bay is denoted by x, positive toward the ocean, and y is positive in the 11°T direction (Fig. 1). The principal component of the flow (the component with largest variance) is u and the transverse component is v. Although the current orientation changes throughout the bay entrance transect, the u component (rotated 11°T) accurately represents inflows and outflows, and the v component reflects flow approximately aligned with the transect. Different rotations of the axes did not affect the essence of the results.

Instantaneous surface flow (u, v) and salinity S values were represented in the space-time domain (Fig. 2) in order to describe the intratidal variations of these parameters, calculate transverse gradients of u, v, and S, and portray the evolution of gradients throughout the four tidal cycles sampled and identify the regions of enhanced gradients along the transect. The space dimension y was assigned as the distance from the southernmost end of the transect off Cape Henry. The time dimension t was the number of hours elapsed after midnight of the day when the experiment commenced. Once u, v, and S were cast in the space-time domain, they were then interpolated onto a uniform grid with Δy of 200 m and Δt of 1 h. Interpolation was carried out through the construction of Delaunay triangulations with the Interactive Data Language (IDL) software. Selected vertical sections of u, v, and S, for each of the two cruises were used to represent the vertical distribution of properties in the area of enhanced gradients.

Wind velocity and sea level were recorded at the Chesapeake Bay Bridge-Tunnel by the National Oceanic and Atmospheric Administration's National Ocean Service and river discharge data were

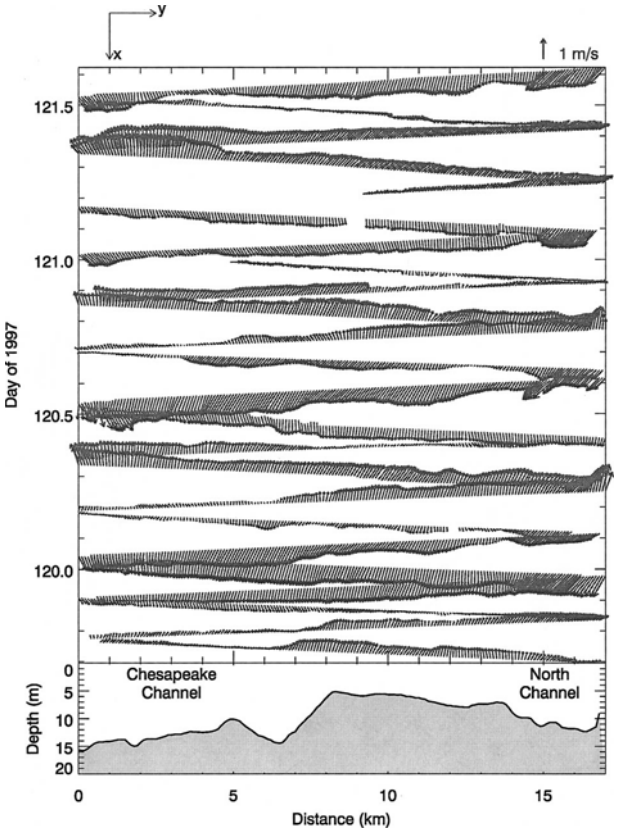

Fig. 2. Instantaneous surface velocities (in the distance-time domain) across the entrance to the Chesapeake Bay at the times of observation during the cruise on April 29–May 1, 1997. Flood flow points upward. The bathymetry of the transect is presented in the lower panel, looking into the estuary.

provided by the United States Geological Survey. The following section presents the wind, sea level, and river discharge conditions that affected the periods of observation, followed by the description of the intratidal flow and salinity variations, and the link of their respective transverse gradients to bathymetry. The linkages were documented with a set of velocity profiles measured across one section at the Chesapeake Bay entrance in the spring and summer of 1997. The dynamical underpinnings of the linkages were explained through examination of the transverse variations of the along-estuary momentum balance, i.e., through a simplified version of the relative vorticity equation.

Results

During the period of observation of April 29–May 1 wind forcing was, for the most part, relatively weak (Fig. 3). The experiment began near the conclusion (the last 4 h) of a northeasterly wind pulse of typical magnitudes of 10 m s^{-1}. During the rest of the experiment, winds were dominated by a southerly component that increased as the experiment progressed. By the end of the experiment the winds were southwesterly at almost 10 m s^{-1}. These southwesterly winds may have produced upwelling off Cape Henry as reflected by a marked increase in surface salinity and decrease in surface temperature. During July 22–24, winds were weaker than in the April–May cruise (Fig. 3) and caused minor effects on u, v, and S. In the April–May cruise, the subtidal sea level showed a decreasing trend, while in the July cruise it tended to increase. The total river discharge into the bay was larger during April–May than during July (Fig. 3c). This was reflected in the different range of salinity variations observed in both cruises as described next.

Intratidal Variability of Salinity and Flow

Surface salinity ranged from 17 to 27 in the April–May cruise and from 24 to 31 in the July cruise (Fig. 4). Flow magnitudes approached 0.9 m s^{-1} in the first cruise (around neap tides) and surpassed 1 m s^{-1} in the second cruise (secondary spring tides). In both cruises, the lowest and highest salinities were usually found off Cape Henry and Fishermans Island, respectively, as expected from the effects of the earth's rotation. One exception occurred toward the end of the first cruise, when the highest salinity was found off Cape Henry, at the southern portion of the entrance (Fig. 4a). The high salinity developed with the onset of flood tidal flow, in contrast to previous flood flows. These high salinity values coincided with low water temperatures at the surface (not shown) and a period of southwesterly winds (Fig. 3), indicative of upwelling off Cape Henry.

In both cruises, the strongest tidal flows appeared over both the Chesapeake and North channels and the weakest flows appeared over Middle Ground—i.e., over the shallow portion between the channels (Fig. 4). The tidal flow over the channels lagged behind the flow over Middle Ground. This distribution of the tidal amplitude and of the phase lags was consistent with those expected from the effects of bottom friction (e.g., Valle-Levinson and Lwiza 1995; Li and Valle-Levinson 1999). The transverse variability of the tidal current amplitudes and phases defined regions of strongest gradients in the flow, which corresponded to the transition between channels and shoals.

During both cruises, surface flow and salinity displayed covariability that was almost 90 degrees out of phase, i.e., extreme salinity values corresponded to periods of slack tidal currents (Fig. 4). This variability suggested the dominance of the advection of the along-estuary salinity gradient by the along-estuary tidal flow in determining the temporal changes in salinity. In general, the lowest salinities

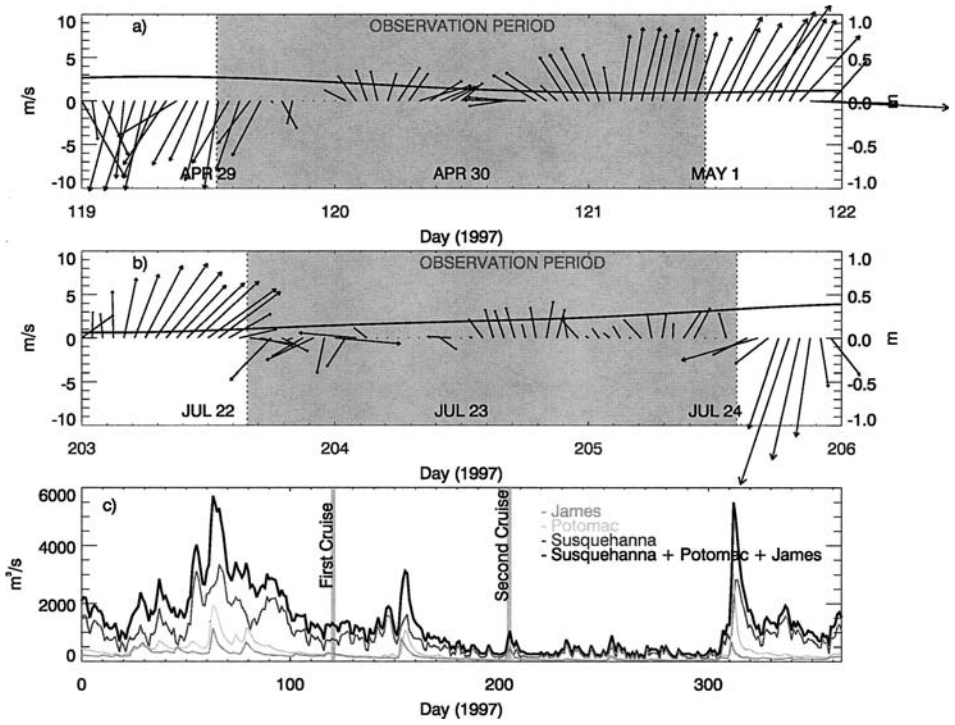

Fig. 3. Meteorological and river discharge conditions during the periods of observation. (a) and (b) indicate wind velocity (vectors) and subtidal sea level (thick line) for the periods April 29–May 1, and July 22–24, respectively. (c) indicates river discharge during 1997 from the three most important rivers.

were restricted to the 8-km wide Chesapeake Channel (Fig. 4). The edge of this channel seemed to delimit the buoyant plume of the bay and reflected the appearance of salinity fronts associated with this plume. On the other hand, the highest salinities were confined to the North Channel during the first three tidal cycles of the first cruise (Fig. 4a). During those three tidal cycles, the southern edge of the North Channel (the left edge looking into the estuary) seemed to limit a branch of high salinity water appearing at the bay entrance. During the second cruise, the highest salinity extended over the entire northern half of the transect. This was likely due to the combination of weaker buoyancy and stronger tidal currents during the July cruise relative to the April–May cruise. The combination of strong tidal and weak buoyancy forcing in July should have allowed the intrusion of high salinity water with every flood period. The linkage among salinity, flow, and bathymetry gradients is explored next through estimation of transverse gradients with the data available.

Flow and Salinity Gradients

To explore linkages among flow, salinity, and bathymetry we calculated transverse gradients of flow (u, v) and salinity S. The transverse gradients were obtained with a forward (in y) discretization scheme. The gradients were represented by 1) $\partial v/\partial y$, denoting divergence of lateral flow, $\partial u/\partial y$, portraying transverse shears of the along-estuary flow, and $\partial S/\partial y$. The divergence of lateral flow $\partial v/\partial y$ may be a reasonable proxy for horizontal divergence in these systems because the divergence of the along-estuary flow $\partial u/\partial x$ tends to be smaller by one order of magnitude (Valle-Levinson et al. 2000). For this particular data set, we cannot assess the influence of $\partial u/\partial x$ on the total divergence, but we acknowledge that this is a source of uncertainty in the representation of divergences.

Divergences

The distribution of $\partial v/\partial y$ in the lower Chesapeake Bay showed distinguishable patterns related to bathymetry changes. These patterns were most marked near the northern end of the transect, i.e., in the North Channel (dark-blue filled contours of Fig. 5). Largest convergence rates lasted between 2 and 3 hours and approached values of 10^{-3} s^{-1} over the slopes of the channel. Looking into the estuary, convergence patterns appeared over the left edge of North Channel (dark-blue filled contours at 15 km) during ebb and over the right edge of the channel (dark-blue filled contours at 17 km) during flood. This alternation persisted during both cruises although not as clearly on the right

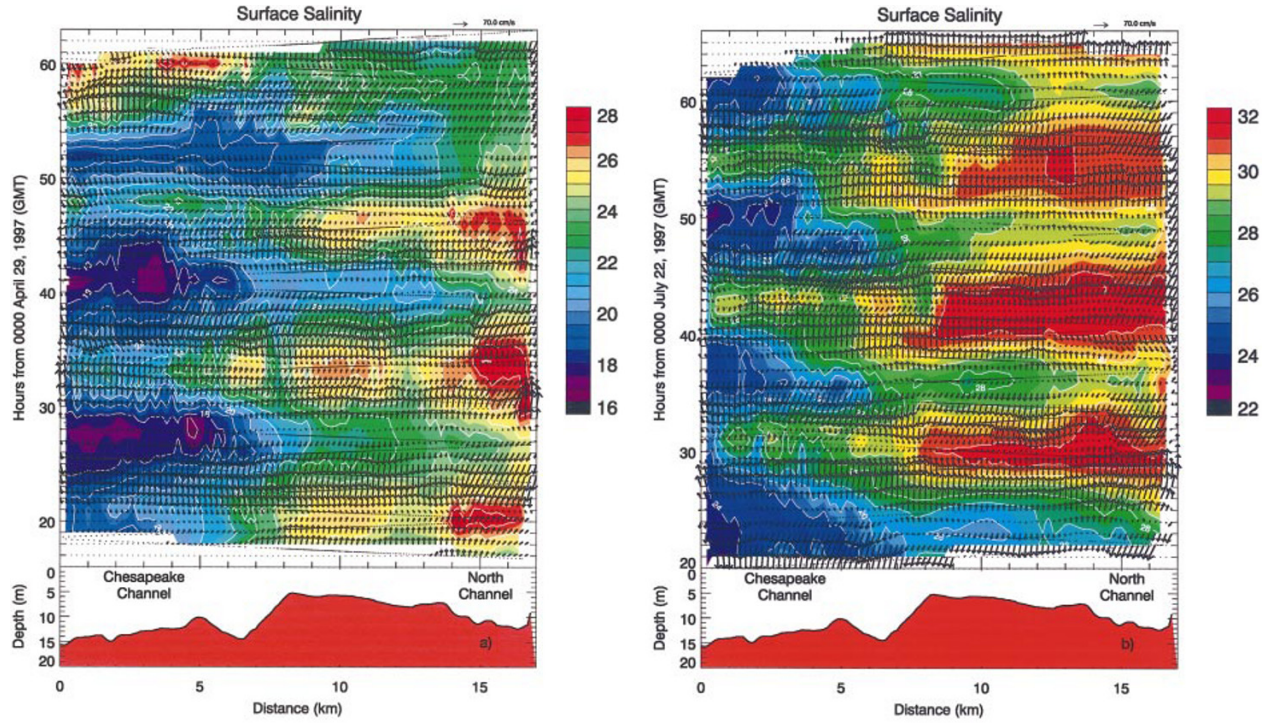

Fig. 4. Surface velocity vectors and salinity (colored contours) interpolated to a uniform time-space grid during both cruises. The white contours indicate salinity at intervals of 1. Closely spaced white dots represent the time and location of each observation. The lower panels represent the bathymetry of the transect sampled. (a) indicates April 29–May 1, 1997, cruise, (b) indicates July 22–24, 1997, cruise. Flood flow points upward.

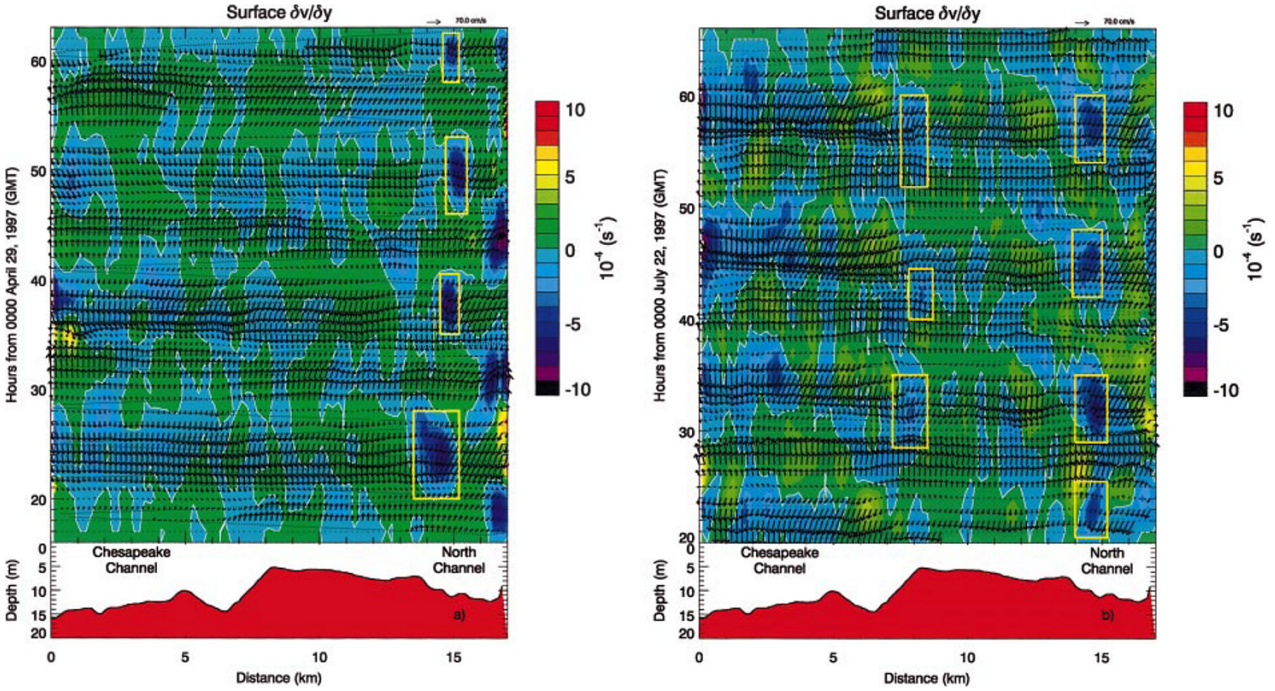

Fig. 5. Surface velocity vectors and divergence rates (colored contours) interpolated to a uniform time-space grid during both cruises. The colored contours denote values of divergence (10^{-4} s^{-1}) at intervals of 1. Blue denotes convergences. The white contours separate positive (divergence) from negative (convergence) values. Flood flow points upward. Yellow rectangles highlight events described in the text. (a) indicates April 29–May 1, 1997, cruise, (b) indicates July 22–24, 1997, cruise.

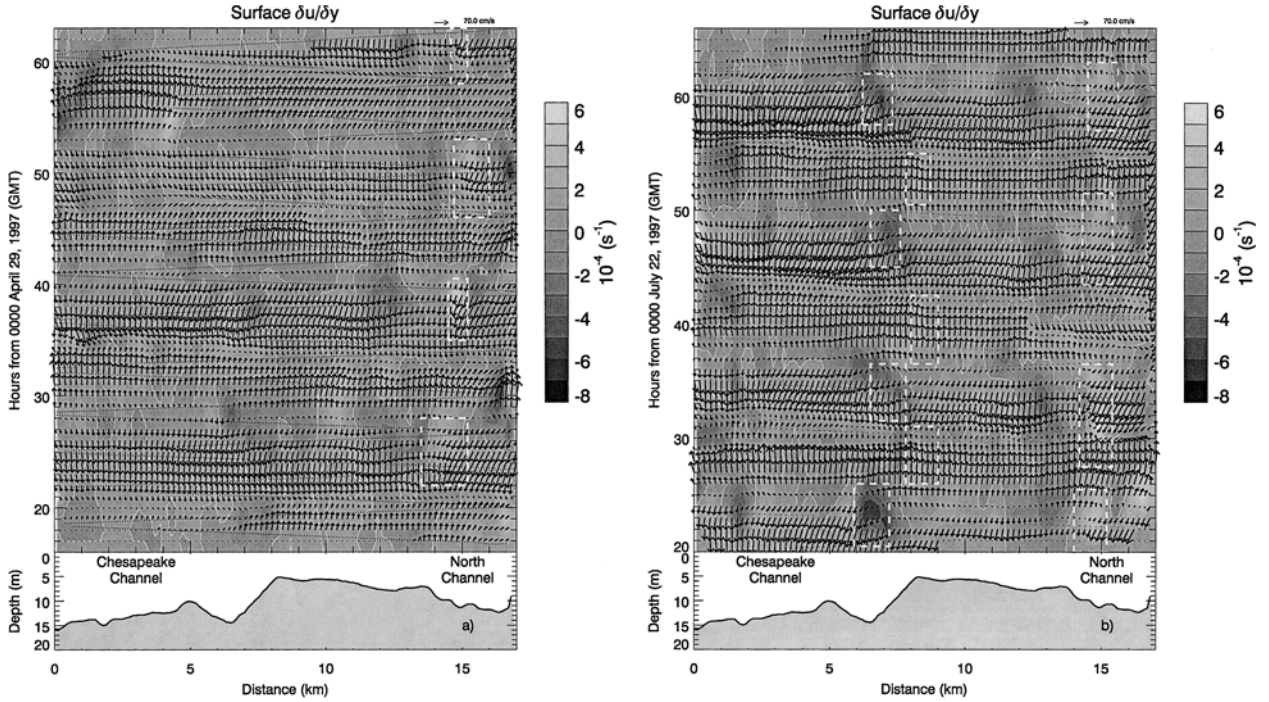

Fig. 6. Surface velocity vectors and transverse shears of the along-estuary tidal flow (shaded contours) interpolated to a uniform time-space grid during both cruises. The shaded contours denote values of shears (10^{-4} s^{-1}) at intervals of 1. The white contours separate positive from negative values. White-dashed rectangles highlight events described in the text. (a) indicates April 29–May 1, 1997, cruise, (b) indicates July 20–22, 1997, cruise. Flood flow points upward.

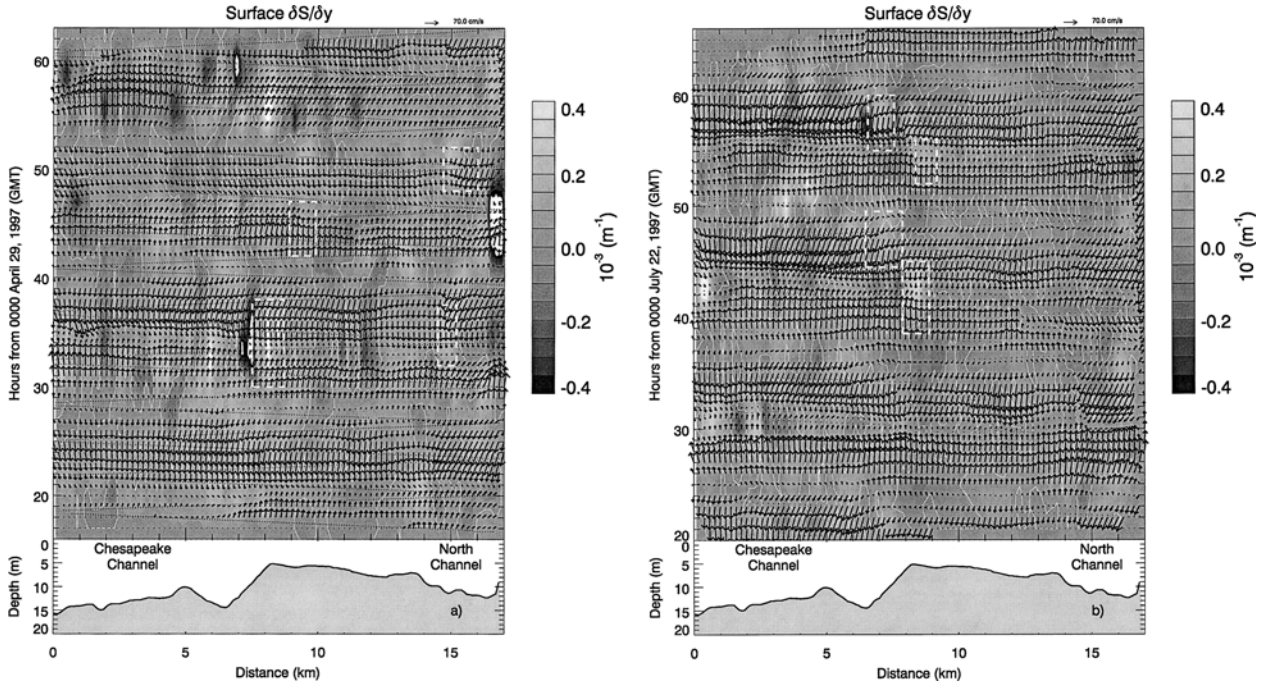

Fig. 7. Surface velocity vectors and transverse gradients in salinity (shaded contours) interpolated to a uniform time-space grid during both cruises. The shaded contours denote gradients (10^{-3} m^{-1}) at intervals of 0.05. The white contours separate positive from negative gradients. White-dashed rectangles highlight events described in the text. (a) indicates April 29–May 1, 1997, cruise, (b) indicates July 20–22, 1997, cruise.

edge of the channel in the second cruise (Fig. 5b) because of lack of measurements across the entire North Channel. Such alternation was also consistent with that observed in the James River by Valle-Levinson et al. (2000). The alternation of convergences from the left edge to the right edge of the channel is considered to be a robust feature attributed to the interaction of tidal flow with bathymetry under the spatially different effects of bottom friction. Bottom friction causes phase lags of the tidal currents from channels to shoals and convergent flows at the channel edges.

Another area of convergences appeared over the northern edge of the Chesapeake Channel (Fig. 5), around 8 km. Convergences were not as strong as over North Channel during the April–May cruise (Fig. 5a), but still they were apparent during late flood to early ebb periods of the July cruise (starting at 30 h, 42 h, and 54 h on Fig. 5b). This was likely favored by weaker buoyancy and stronger tidal forcing in the July cruise relative to the April–May cruise. In general, the area of convergences over the northern edge of Chesapeake Channel was closely linked to the outer edge of the Chesapeake Bay outflow plume (Sletten et al. 1999). The ebb convergences observed around 2 km in the July cruise were likely an effect of the confluence of Thimble Shoal and Chesapeake Channels.

Transverse Shears

The areas of strongest convergence in Fig. 5 were linked to large transverse shears in the along-estuary flow $\partial u/\partial y$ (Fig. 6). The distributions of $\partial u/\partial y$ during the first cruise showed very similar alternations over the North Channel (light-shaded contours on Fig. 6a) as the pattern of convergences (Fig. 5a). Large positive shears, close to 5×10^{-4} s^{-1}, were clearly observed during ebb flows over the left slope of the North channel (looking into the estuary). This meant that the ebb flow increased rapidly from the shoal to the channel due to less bottom friction in the channel. Analogous linkages between $\partial u/\partial y$ and $\partial v/\partial y$ over North Channel were observed in the July cruise (Fig. 6b).

Consistently with the distribution of convergences over the northern edge of the Chesapeake Channel there was no apparent regular pattern of transverse shears at this location during the first cruise (km on Fig. 6a). In agreement with the convergences in this area, there was a regular pattern of shears during the July cruise (Fig. 6b). In July, enhanced positive shears (light-shaded contours) appeared during flood at approximately 8.2 km and at 30 h, 42 h, and 54 h, as the tidal currents (negative) decreased from the channel to the shoal. Increased negative shears (dark shaded contours) appeared during ebb at approximately 7.5 km and at 22 h, 34 h, 47 h, and 60 h as the tidal currents (positive) decreased from the channel to the shoal. This distinct behavior over the Chesapeake Channel from the first to the second cruise was attributed, once more, to the weakened buoyancy and stronger tidal currents during the second cruise that allowed a tighter frictional coupling between tidal currents and bathymetry.

Transverse Salinity Gradients

The transverse salinity gradients were sometimes related to the flow gradients. During the first cruise, increased salinity gradients were found over the left slope of North Channel (~15 km) during the second and third ebb cycles, i.e., at 35 and 50 h (light-shaded contours on Fig. 7a). These two frontal regions were closely related to large convergences and transverse shears (Figs. 5a and 6a). The interesting feature of these two fronts was that salinity increased in the channel, relative to the adjacent shoals, during ebb. This increase was contrary to the decrease expected from the greater advection of fresher waters, relative to the regions outside of the channel, by stronger ebb currents (e.g., Nunes and Simpson 1985; Huzzey and Brubaker 1988). Below, we shall examine the vertical structure of one of these fronts, the one at 50 h, and offer a possible reason for this increase of salinity in the channel during ebb. During the July cruise, salinity increases also appeared in North Channel. This time, the increment appeared close to the right edge of the channel and by the end of ebb (Fig. 7b). Furthermore, these increases were not related to enhanced flow gradients (see Figs. 5b and 6b).

Over the northern edge of Chesapeake Channel there were no clear tidal alternations of salinity gradients during the first cruise. Nonetheless, strong gradients appeared concentrated between 7 and 9 km (light- and dark-shaded contours on Fig. 7a). This distance was equivalent to the internal radius of deformation obtained from the product of the buoyancy frequency (N equals $\sqrt{-(g/\rho)(\partial\rho/\partial z)}$, where g is the acceleration due to gravity, ρ is water's density, and z is the vertical coordinate, positive upward) times the water column depth H, divided by the Coriolis parameter f. During the first cruise, N was typically 0.077 s^{-1} over a depth of 9 m, which gave a radius of deformation of 8 km, in the middle of the location of marked frontal features (Fig. 7a). These fronts were related to the Chesapeake Bay outflow plume and were probably isolated from bathymetric influences because their timing was not related to the tidal flow interacting with bathymetry gradients as observed over the North Channel. There were two instances, however, when large salinity gradients

coincided with increased convergences. One was at a distance of 8 km and around 35 h, during ebb, and the other one at a distance of 9.3 km and around 45 h, at the end of flood (Figs. 5a and 7a). In the latter instance, the salinity gradients and the convergences were also related to increased transverse shears (Fig. 6a). This linkage developed over the shallow Middle Ground and did not coincide with a bathymetric gradient. During the second half of the second cruise the coupling among gradients in bathymetry, tidal flow, and salinity was more evident than in the first cruise (Fig. 7b). Enlarged gradients appeared by the end of flood over the northern edge of Chesapeake Channel, at a distance of 8.5 km, and at 43 h and 54 h, which were linked to increased $\partial u/\partial y$ (Fig. 6b) and negative $\partial v/\partial y$ (Fig. 5b). Similarly, increased salinity gradients in late ebb developed twice, at a distance of 7.3 km and at 47–48 h and 59 h, concurrently with enlarged negative $\partial u/\partial y$ but under weak convergences. As mentioned above, buoyancy was less and tidal forcing was stronger than during the April–May cruise. The different forcings could have allowed the surface tidal flow, modified by the bathymetry, to modulate the position of the plume, at least during the second half of the cruise, which was when the modulation was apparent. This linkage produced by the tidal flow interacting with bathymetry and the salinity field was further explored by examining the vertical structure of the flow and salinity fields at two selected fronts that developed over North Channel, one during each cruise.

Fronts Over North Channel

The first front examined appeared at a distance of 15 km and at 50 h soon after maximum ebb during the first cruise (Figs. 5a, 6a, and 7a). The vertical structure of u at the front over North Channel showed marked transverse shears throughout the water column (Fig. 8). The region of strongest transverse shears, as denoted by the closely spaced contours, migrated from the channel's slope toward the channel's edge as distance from the surface increased. The small bump in the middle of the channel, at 15 km, partitioned the tidal outflow below 5 m as indicated by the isotachs. Similar spatial variations could be noticed for the transverse flow, which showed marked convergences associated with the region of strong transverse shears (Fig. 8). It is noteworthy that the transverse flows associated with the convergences were in the same direction throughout the water column in contrast to the proposed helicoidal transverse circulation resulting from axial convergences (Nunes and Simpson 1985), but in agreement with observations in the James River (Valle-Levinson et al. 2000). Secondary circulation developed within the first 5 km of the Chesapeake Channel during late ebb (upper panel of Fig. 8) and early flood (lower panel of Fig. 8). This type of flow has been attributed to curvature effects around a headland (e.g., Geyer 1993), i.e., around Cape Henry in this case.

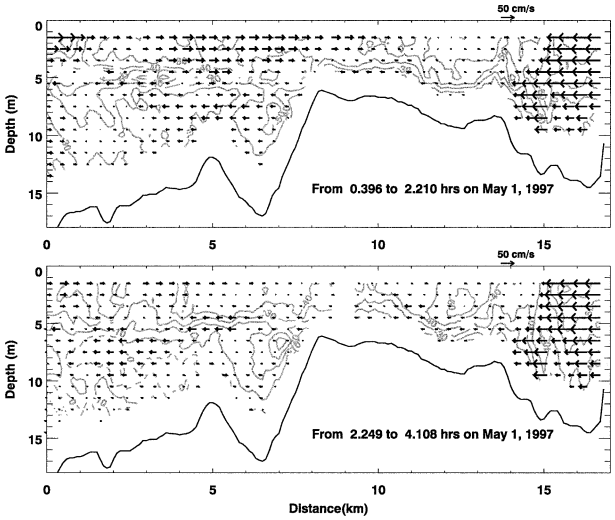

Fig. 8. Vertical sections, looking into the estuary, of along-estuary (contours) and across-estuary (vectors) flow during ebb on May 1, 1997. Contour interval is 10 cm s^{-1}. The upper panel was sampled from left to right and the lower panel from right to left.

The flow gradients observed at 50 h in the April–May cruise were linked to a marked salinity front at 15 km that extended throughout the water column (Fig. 9). Two branches of high salinity water coincided with the outflow bifurcation over the lower half of the water column. The concurrence of flow and salinity gradients indicated that the salinity front was produced by the greater advection, relative to the region outside of the channel, of high salinity water from an upstream location. This mechanism had not been reported as causative of along-estuary fronts. The mechanism of differential advection of the density field by the tidal currents (e.g., Nunes and Simpson 1985; Huzzey and Brubaker 1988) would have predicted flow divergence and low salinity in the channel, contrary to our observations. As seen from the surface salinity variations throughout the 4 tidal cycles observed in the April–May cruise (Fig. 4a), relatively higher salinity persisted in the channel with respect to the adjacent shoal. This probably resulted from the location of the channel where Coriolis accelerations favor intrusion of high salinity water into the Chesapeake Bay. The transverse structure of the along estuary density gradient also should play a role in the formation of these fronts. Our sampling did not resolve along-estuary gradients so we could not

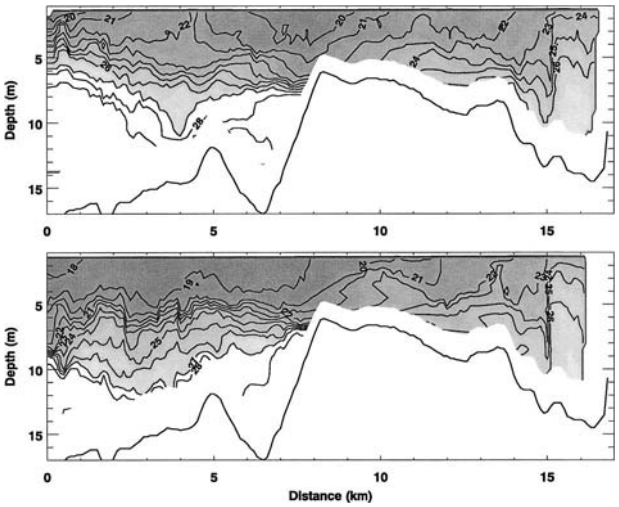

Fig. 9. Same as Fig. 8 but for salinity fields. Contour interval is 1.

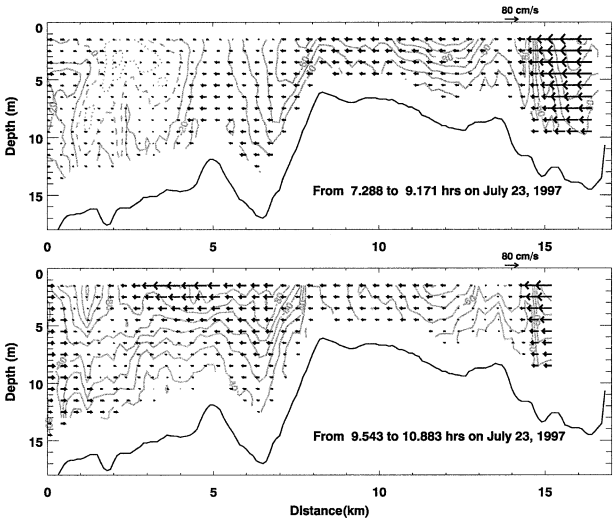

Fig. 10. Vertical sections, looking into the estuary, of along-estuary (contours) and across-estuary (vectors) flow during ebb on July 23, 1997. Contour interval is 10 cm s^{-1}. The upper panel was sampled from left to right and the lower panel from right to left.

determine the relative importance of this mechanism.

The second front examined appeared at a distance of 14.7 km and at 33 h of the July cruise, also during ebb tidal flow (Figs. 5b, 6b, and 7b). In this case, the region of strongest transverse shears of u over North Channel extended roughly straight down from surface to bottom (Fig. 10). The southern edge of North Channel (between 13 and 14 km) markedly dampened the outflow, analogous to the northern edge of Chesapeake Channel (between 8 and 9 km), and allowed the development of large transverse shears. Strong convergences of lateral flow also appeared over these regions, most appreciably in the North Channel. Also noteworthy was the secondary circulation around Cape Henry, within 4 km inside the Chesapeake Channel, that appeared only in late flood-early ebb (upper panel of Fig. 10). The salinity front linked to the flow gradients over the North Channel was not as dramatic as the one in the April–May cruise but still was apparent (Fig. 11). The front was produced by the outflow of low salinity water, in contrast to the first cruise, in the form of a buoyant wedge. Although the transverse shears and convergences were practically depth-independent (Fig. 10) the salinity gradients showed appreciable depth-dependence. This buoyant wedge was explained by the differential advection of the density field by the tidal currents (Huzzey and Brubaker 1988) as clearly seen through the comparison of Figs. 10 and 11 over the region to the north of 10 km. The differential advection mechanism would have predicted divergence not convergence. This is perhaps owing to a stronger linkage between transverse shears and convergences in the formation of along-estuary fronts, rather than between density field and convergences (Valle-Levinson et al. 2000). We also propose here that the dynamic linkage between transverse shears and convergences occurs through the vertical component of vorticity as explored next.

Linkages through Vorticity

The vertical component of the vorticity relative to a rotating frame $\partial v/\partial x - \partial u/\partial y$ may be expanded through cross-differentiation of the horizontal momentum equations:

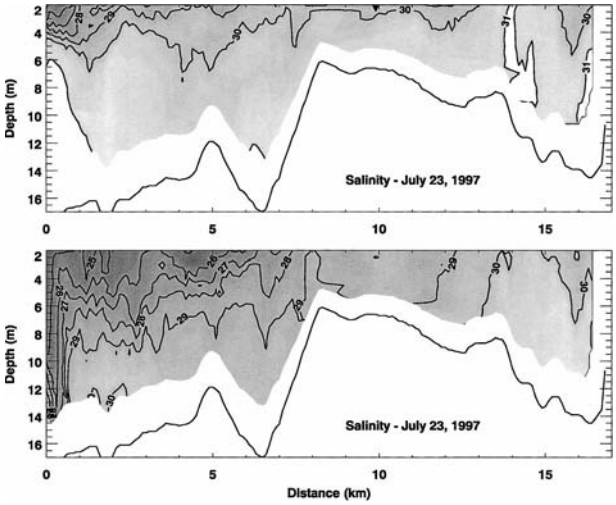

Fig. 11. Same as Fig. 8 but for salinity fields. Contour interval is 1.

$$\frac{\partial}{\partial y}\left(\frac{\partial u}{\partial t} + u\frac{\partial u}{\partial x} + v\frac{\partial u}{\partial y} + w\frac{\partial u}{\partial z} - fv = -g\frac{\partial \eta}{\partial x} - \frac{g}{\rho}\int_{-z}^{0}\frac{\partial \rho}{\partial x}\,dz + Friction_x\right) \quad (1)$$

$$\frac{\partial}{\partial x}\left(\frac{\partial v}{\partial t} + u\frac{\partial v}{\partial x} + v\frac{\partial v}{\partial y} + w\frac{\partial v}{\partial z} + fu = -g\frac{\partial \eta}{\partial y} - \frac{g}{\rho}\int_{-z}^{0}\frac{\partial \rho}{\partial y}\,dz + Friction_y\right) \quad (2)$$

where f is the Coriolis parameter (s^{-1}), η is surface elevation (m), ρ is water density (m s), g is the acceleration due to gravity (9.8 m s), and w is the vertical velocity component (m s^{-1}). Differentiation of Eq. 1 and Eq. 2 and subtraction yields, after some algebra:

$$\frac{d\zeta}{dt} + v\frac{\partial f}{\partial y} + f\left(\frac{\partial u}{\partial x} + \frac{\partial v}{\partial y}\right) + \zeta\left(\frac{\partial u}{\partial x} + \frac{\partial v}{\partial y}\right) = -\frac{\partial}{\partial x}\left(\frac{g}{\rho}\int_{-z}^{0}\frac{\partial \rho}{\partial y}\,dz\right) + \frac{\partial}{\partial y}\left(\frac{g}{\rho}\int_{-z}^{0}\frac{\partial \rho}{\partial x}\,dz\right) + \frac{\partial}{\partial x}(Friction_y) - \frac{\partial}{\partial y}(Friction_x) \quad (3)$$

(e.g., Gill 1982, section 7.10; Pedlosky 1979, section 2.4 for the left-hand side of Eq. 3, where ζ is the relative vorticity $\partial v/\partial x - \partial u/\partial y$). The differentials with respect to x may be neglected if the along-estuary gradients are one or more orders of magnitude smaller than the across-estuary gradients, which was likely the case here. Then, the absolute vorticity ζ_A may be re-written as $f + \tilde{\zeta} = f - (\partial u/\partial y)$, and Eq. 3 becomes:

$$\frac{d\zeta_A}{dt} + \zeta_a\frac{\partial v}{\partial y} = \frac{\partial}{\partial y}\left(\frac{g}{\rho}\int_{-h}^{0}\frac{\partial \rho}{\partial x}\,dz\right) - \frac{\partial}{\partial y}(Friction_x) \quad (4)$$

And solving for $\partial v/\partial y$, which represents a proxy for the divergence of the flow, yields:

$$\frac{\partial v}{\partial y} = -\frac{1}{\zeta_A}\frac{\partial \zeta_A}{\partial t} + \frac{1}{\zeta_A}\frac{\partial}{\partial y}\left(\frac{g}{\rho}\int_{-h}^{0}\frac{\partial \rho}{\partial x}\,dz\right) - \frac{1}{\zeta_A}\frac{\partial}{\partial y}(Friction_x) \quad (5)$$

Note that the first term in the right-hand side of Eq. 5, which represents the local temporal changes of absolute vorticity, has been linearized (relative to Eq. 4) as suggested by Mied et al. (2000). Near-surface observations of $\partial u/\partial y$ in the North Channel (15 km) from two cruises in the lower Chesapeake Bay were used to assess that term, which was the one that could be most reliably evaluated. The

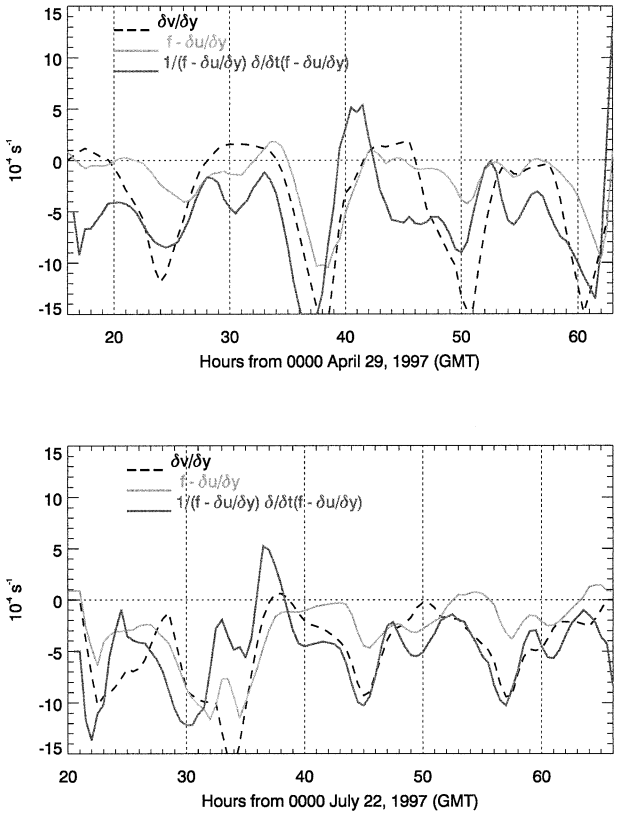

Fig. 12. Values of $\partial v/\partial y$, $f - \partial u/\partial y$, and the local contribution to the first term on the right-hand side of Eq. 5. The advective contribution to the temporal changes of the absolute vorticity has been neglected. The lines represent the maximum value, at any given time, that appeared between 14.6 and 15 km. (a) indicates April 29–May 1, 1997, cruise, (b) indicates July 20–22, 1997, cruise.

second term in the right-hand side of Eq. 5 represented the transverse variability of the along-estuary density gradient, and the third term depicted the transverse variability in friction. In Fig. 12, we compare the values of $\partial v/\partial y$ to those of ζ_A (alone) and the first term on the right-hand side of Eq. 5. The values of $\partial v/\partial y$ were closely followed by the values of ζ_A and by the local changes of the absolute vorticity. The similarity between $\partial v/\partial y$ and the changes in absolute vorticity was maximized by a constant offset of 4×10^{-4} s^{-1}, which should have represented a bias in the estimates and the combined contribution of the transverse variability of density gradients and friction to the convergence rates. Nonetheless, the first term on the right hand side of Eq. 5 reproduced well the timing of the convergences. This relationship indicated a tight coupling between transverse shears and convergence rates as alternatively proposed by Mied et al. (2000, p. 8654) through the ''tilting of planetary vorticity.'' The other two terms on the right hand

side of Eq. 5 should conceptually contribute to the convergences, as pointed out by Nunes and Simpson (1985) for the transverse variability in the density field, and by Bowman and Iverson (1977) for the transverse variability in mixing. The relative contribution of these two mechanisms, as well as that from the advection of vorticity, remains to be elucidated. The present analysis (Fig. 12) did indicate that the convergence rates were closely linked to the transverse shears of the along-estuary flows, through the absolute vorticity. The transverse shears, which were of similar magnitude to that of the convergences, were linked to the areas of bathymetry changes, as demonstrated analytically by Li and Valle-Levinson (1999).

Summary

The strongest flow convergences alternated over the left and right slopes of the North Channel (looking into the estuary) during ebb and flood periods, respectively. These gradients in flow and bathymetry were linked to strong transverse shears in the along-estuary flow and to fronts in the salinity field. The linkage was best defined over the left slope of the channel during ebb periods. The transverse shears of the along-estuary tidal flow were produced by lateral differences in tidal current amplitude and phase triggered by transverse bathymetry changes. Through the vorticity equation, we propose that there are three mechanisms that may explain convergences/divergence patterns: linkage through the transverse shears of the along-estuary flow; linkage through lateral variations of the along-estuary density gradient; and linkage through lateral variations of frictional forces. The observations obtained in this study allowed evaluation of the first mechanism, which appeared to reproduce the timing and approximate magnitude of the convergences. It is proposed to be a crucial mechanism that produced fronts in areas of strong coupling between tidal flows and bathymetry. The other two mechanisms should influence the magnitude of the convergences and require further evaluation.

Acknowledgments

This study was funded by the U.S. National Science Foundation as part of the Land-Margin Ecosystem Research in the Chesapeake Bay. The study Trophic Interaction in Estuarine Systems (ITES) was funded under NSF Award DEB19412133. AVL acknowledges funding from NSF Award 9529806 that allowed him to participate in the LMER project. We appreciate the dedication of the crew of the R/V *Cape Henlopen* and the efforts in data collection and preliminary processing by Lorraine Brasseur (formerly Heilman) and Cathy Lascara. This is UMCES Contribution # 3629.

Literature Cited

Bowman, M. J. and R. L. Iverson. 1977. Estuarine and plume fronts, p. 87–104. *In* M. J. Bowman and W. E. Esaias (eds.), Oceanic Fronts in Coastal Processes. Springer-Verlag, Berlin, Germany.

Brown, J., W. R. Turrell, and J. H. Simpson. 1991. Aerial surveys of axial convergent fronts in UK estuaries and the implications for pollution. *Marine Pollution Bulletin* 22:397–400.

Browne, D. R. and C. W. Fisher. 1988. Tide and tidal currents in the Chesapeake Bay. NOAA Technical Report NOS OMA 3. U.S. Department of Commerce, Rockville, Maryland.

Brubaker, J. M. and J. H. Simpson. 1999. Flow convergence and stability at a tidal estuarine front: Acoustic Doppler current observations. *Journal of Geophysical Research* 104:18,257–18,268.

Ferrier, G. and J. M. Anderson. 1997. A multi-disciplinary study of frontal systems in the Tay estuary, Scotland. *Estuarine, Coastal and Shelf Science* 45:317–336.

Garvine, R. 1974. Dynamics of small-scale ocean fronts. *Journal of Physical Oceanography* 4:557–569.

Geyer, W. R. 1993. Three-dimensional tidal flow around headlands. *Journal of Geophysical Research* 98:955–966.

Gill, A. E. 1982. Atmosphere-Ocean Dynamics. Academic Press, San Diego, California.

Huzzey, L. M. and J. M. Brubaker. 1988. The formation of longitudinal fronts in a coastal plain estuary. *Journal of Geophysical Research* 93:1329–1334.

Joyce, T. M. 1989. On in situ calibration of shipboard ADCPs. *Journal of Atmospheric and Oceanic Technology* 6:169–172.

Li, C. and A. Valle-Levinson. 1999. A 2-D analytic tidal model for a narrow estuary of arbitrary lateral depth variation: The intra-tidal motion. *Journal of Geophysical Research* 104:23,525–23,543.

Luketina, D. A. and J. Imberger. 1989. Turbulence and entrainment in a buoyant surface plume. *Journal of Geophysical Research* 94:12,619–12,636.

Marmorino, G. O. and C. L. Trump. 1996. High-resolution measurements made across a tidal intrusion front. *Journal of Geophysical Research* 101:25,661–25,674.

Mied, R. P., R. A. Handler, and T. E. Evans. 2000. Longitudinal convergence fronts in homogeneous rotating channels. *Journal of Geophysical Research* 105:8647–8658.

Nunes, R. A. and J. H. Simpson. 1985. Axial convergence in a well-mixed estuary. *Estuarine, Coastal and Shelf Science* 20:637–649.

O'Donnell, J. 1993. Surface fronts in estuaries: A review. *Estuaries* 16:12–39.

O'Donnell, J. 1997. Observations of near-surface currents and hydrography in the Connecticut River plume with the surface current and density array. *Journal of Geophysical Research* 102: 25,021–25,033.

O'Donnell, J., G. O. Marmorino, and C. L. Trump. 1998. Convergence and downwelling at a river plume front. *Journal of Physical Oceanography* 28:1481–1495.

Paraso, M. and A. Valle-Levinson. 1996. Atmospheric forcing effects on sea level and water temperature in the lower Chesapeake Bay: 1992. *Estuaries* 19:548–561.

Pedlosky, J. 1979. Geophysical Fluid Dynamics. Springer-Verlag, New York.

Sarabun, C. C. 1980. Structure and formation of Delaware Bay fronts. Ph.D. Dissertation, The University of Delaware, Newark, Delaware.

Simpson, J. H. and W. R. Turrell. 1986. Convergent fronts in the circulation of tidal estuaries, p. 139–152. *In* D. A. Wolfe (ed.), Estuarine Variability. Academic Press, Orlando, Florida.

Sletten, M. A., G. O. Marmorino, T. F. Donato, D. J. McLaughlin, and E. Twarog. 1999. An airborne, real aperture radar study of the Chesapeake Bay outflow plume. *Journal of Geophysical Research* 104:1211–1222.

Swift, M. R., D. W. Fredriksson, and B. Celikkol. 1996. Struc-

ture of an axial convergence zone from acoustic Doppler current profiler measurements. *Estuarine, Coastal and Shelf Science* 43:109–122.

TURRELL, W. R., J. BROWN, AND J. H. SIMPSON. 1996. Salt intrusion and secondary flow in a shallow, well-mixed estuary. *Estuarine, Coastal and Shelf Science* 42:153–169.

VALLE-LEVINSON, A., C. LI, T. ROYER, AND L. ATKINSON. 1998. Flow patterns at the Chesapeake Bay entrance. *Continental Shelf Research* 18:1157–1177.

VALLE-LEVINSON, A., C. LI, K. C. WONG, AND K. M. M. LWIZA. 2000. Convergence of lateral flow along a coastal plain estuary. *Journal of Geophysical Research* 105:17,045–17,061.

VALLE-LEVINSON, A. AND K. M. M. LWIZA. 1995. Effects of channels and shoals on the exchange between the lower Chesapeake Bay and the adjacent ocean. *Journal of Geophysical Research* 100:18,551–18,563.

VALLE-LEVINSON, A. AND J. O'DONNELL. 1996. Tidal interaction with buoyancy driven flow in a coastal plain estuary, p. 265–281. *In* D. G. Aubrey and C. T. Friedrichs (eds.), Buoyancy Effects on Coastal and Estuarine Dynamics, Coastal Estuarine Study, Volume 53. AGU, Washington, D.C.

Received for consideration, April 15, 2002
Revised, December 6, 2002
Accepted for publication, January 13, 2003